Observed Trends and Teleconnections of the Siberian High: A Recently Declining Center of Action

FOTIS PANAGIOTOPOULOS AND MARIA SHAHGEDANOVA

Department of Geography, University of Reading, Reading, United Kingdom

ABDELWAHEB HANNACHI AND DAVID B. STEPHENSON

Department of Meteorology, University of Reading, Reading, United Kingdom

(Manuscript received 16 June 2003, in final form 13 September 2004)

ABSTRACT

This study investigates variability in the intensity of the wintertime Siberian high (SH) by defining a robust SH index (SHI) and correlating it with selected meteorological fields and teleconnection indices. A dramatic trend of –2.5 hPa decade^{-1} has been found in the SHI between 1978 and 2001 with unprecedented (since 1871) low values of the SHI. The weakening of the SH has been confirmed by analyzing different historical gridded analyses and individual station observations of sea level pressure (SLP) and excluding possible effects from the conversion of surface pressure to SLP.

SHI correlation maps with various meteorological fields show that SH impacts on circulation and temperature patterns extend far outside the SH source area extending from the Arctic to the tropical Pacific. Advection of warm air from eastern Europe has been identified as the main mechanism causing milder than normal conditions over the Kara and Laptev Seas in association with a strong SH. Despite the strong impacts of the variability in the SH on climatic variability across the Northern Hemisphere, correlations between the SHI and the main teleconnection indices of the Northern Hemisphere are weak. Regression analysis has shown that teleconnection indices are not able to reproduce the interannual variability and trends in the SH. The inclusion of regional surface temperature in the regression model provides closer agreement between the original and reconstructed SHI.

1. Introduction

Inspection of monthly winter sea level pressure (SLP) maps reveals the existence of an extensive semipermanent anticyclone over Asia. It can clearly be seen as a maximum in the winter mean SLP in the Northern Hemisphere (NH; Fig. 1). This feature, known as the Siberian high (SH), is associated with the coldest and densest air masses in the Northern Hemisphere (Lydolf 1977). It is a semipermanent and quasi-stationary atmospheric center of action, dominant in the boreal winter season. The SH forms generally in October mainly in response to strong and continuous radiative cooling in the lower troposphere above the snow-covered surface of Asia and persists until around the end of April. Lydolf (1977) considered the SH to be a shallow cold-core system confined to the lower levels of the troposphere below the 500-hPa pressure level. The SH is usually centered over northern Mongolia but often spreads over a very large part of Asia, thereby dominating low-level circulation in that area in winter (Fig. 1).

Despite its prominence and large spatial extent, surprisingly little is known about the temporal variability of the SH and its possible nonlocal impacts on weather and climate in the NH. Most previous studies have tended to focus on variability in other centers of action such as the Icelandic and Aleutian lows related to the North Atlantic and North Pacific Oscillations, respectively (Stephenson et al. 2002; Panagiotopoulos et al. 2002).

However, the local effects of the SH in weather and climate in Asia have been documented. Large parts of central and eastern Siberia are under the direct influence of the SH and experience extremely cold and dry conditions associated with the minimal cloud cover and the longwave radiation losses (Lydolf 1977). By contrast, the possible role of the SH in climatic variability over Europe and the Arctic region has received relatively little attention. Rogers (1997) studied the North Atlantic storm-track variability and suggested that a westward extension of the SH into Europe is associated

Corresponding author address: Fotis Panagiotopoulos, Dept. of Geography, University of Reading, Whiteknights, Reading RG6 6AB, United Kingdom.
E-mail: f.panagiotopoulos@reading.ac.uk

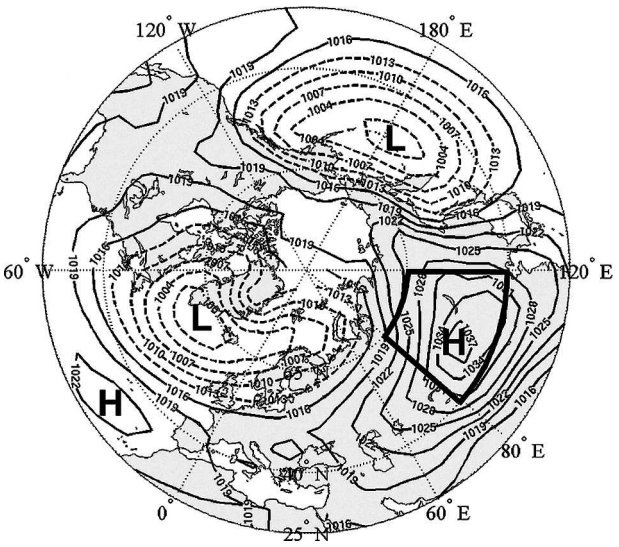

FIG. 1. Winter (DJF) SLP averaged over 1900–2001 using the Trenberth and Paolino (1980) gridded SLP dataset. Isobars are spaced every 3 hPa with solid contours used for SLP values greater or equal than 1015 hPa and dashed lines used for lower values. The area enclosed by the bold line shows the region over which SLP has been averaged to calculate the SH index (40°–65°N, 80°–120°E).

with southwesterly advection of warm air into northern Europe.

The few published studies on the temporal variability of the SH are often contradictory. Sahsamanoglou et al. (1991) studied the climatological aspects and temporal variability of the SH by analyzing a 116-yr record (1873–1988) of observational SLP data compiled by Jones (1987). Sahsamanoglou et al. (1991) constructed an index based on the maximum value of SLP for each month and found a gradual weakening of the SH after 1970. They related the decrease in the intensity of the SH to the continuous warming of the lower troposphere observed over Siberia during the same period. This result, however, was not confirmed by the observational study of Mokhov and Petukhov (1999), who found instead an intensification of the SH since 1960. Their study was based on SLP data derived from synoptic charts. Such data are known to contain errors, but it is not clear whether the difference in results between Sahsamanoglou et al. (1991) and Mokhov and Petukhov (1999) is solely a result of data quality. To our knowledge, no other research has been published on this important issue, leaving unanswered the question about the existence of any long-term trends in the intensity of the SH. Observed historical trends in the SH intensity were also not explicitly addressed by Houghton et al. (2001).

Investigation of the relationship between the SH and Eurasian snow cover has received attention but has also produced inconclusive results. Clark et al. (1999) found no significant impact of the SH variability on temperature variability in Europe in their study of relationships between snow extent, atmospheric circulation and temperature over Eurasia. However, Cohen and Entekhabi (1999) linked changes in Eurasian snow cover extent with variability in the extent of the SH. They argued that during years with extensive autumn and winter snow cover in Eurasia, the SH expands initially westward into northern Europe and then northward over the frozen Arctic into North America, bringing unusually cold air in these regions.

The published literature raises two important and unanswered questions: 1) What are the historical trends in the intensity of the SH? 2) How is SH variability related to climatic variability elsewhere in the extratropical regions of the Northern Hemisphere?

This study addresses these two questions by analyzing historical gridded and station monthly mean SLP datasets, which are briefly described in section 2. An area-averaged index of the SH (SHI) is also presented in this section. Temporal variability and trends in the SH intensity are discussed in section 3. In section 4, teleconnections are investigated in the NH using the SHI, and the relationship of the SHI with major teleconnection patterns is discussed. Conclusions are presented in section 5.

2. Data and methods

a. Data

The SH is best defined using SLP rather than other fields such as 500-hPa geopotential height because of its predominantly thermal nature and small vertical depth. This study makes use of wintertime [December–January–February (DJF)] means of both historical gridded analyses of SLP and individual station observations of SLP and surface pressure. To assess the effect of poor interpolation due to missing data or statistical corrections applied to the datasets, three different gridded SLP datasets have been analyzed and compared. All three datasets consist of monthly means of SLP, and their details are summarized in Table 1.

In addition to pressure data, globally gridded monthly means of various other meteorological variables for 1948–2001 obtained from the National Centers for Environmental Prediction–National Center for

TABLE 1. Details of gridded SLP datasets used in this study [available online at http://dss.ucar.edu/datasets/ds010.1/ (Trenberth and Paolino 1980), http://www.cru.uea.ac.uk/cru/data/pressure.htm (Jones 1987), and from the Met Office's Hadley Centre (Allen et al. 1996; GMSLP2)].

Name	Period	Resolution (lat × lon)	Comments
Trenberth	1899–2001	5° × 5°	Statistical corrections before 1922
Jones	1873–2000	5° × 10°	
GMSLP2	1871–1994	5° × 5°	A blend of observational and modeled data

Atmospheric Research (NCEP–NCAR) reanalyses have also been used (available online at http://www.cpc.ncep.noaa.gov/products/wesley/reanalysis.html).

Surface pressure and SLP for several individual stations have also been analyzed for the available data period of 1922–98. Table 2 provides information about the stations and periods with missing data. The locations of the stations are shown in Fig. 2. The reliability of the gridded datasets was tested by comparing with station observations of SLP and surface pressure (available from NCAR). Correlations between SLP values of the gridded datasets at single grid points in the source area of the SH and observations from stations located very close to these grid points were calculated (not shown). The correlations were highest for the Global Mean SLP (GMSLP2) and Trenberth datasets.

b. Defining an SH index

Area-averaged indices are usually more reliable and can provide more insight than single-point indices such as those used by Sahsamanoglou et al. (1991) and Mokhov and Petukhov (1999). This is because errors at single locations get averaged out and because the area-averaged indices represent variability in a *center of action* rather than at a single location only. An SHI was created by averaging SLP over the key region between 40°–65°N and 80°–120°E for each gridded dataset (Fig. 1). The geographical region was carefully chosen by preparing and examining an atlas of monthly maps of SLP for all winter months between 1871 and 2001 (392 in total). Examination of the atlas revealed that the SH dominated this area with the exception of a few months only (e.g., February 1986 and January 1971). The SH sometimes extends south of 40°N, however, this region is characterized by complex and high terrain, and problems can then arise when extrapolating surface pressure to SLP.

To verify the area-averaged index, a station-based SHI was also constructed by taking the mean of the SLP station observations for the period 1922–98 from the 11 selected stations located within the same geographical domain (Table 2 and Fig. 2). Because of missing data, 3 stations were used for the period 1922–41, 7 stations were used for the period 1922–51, and 11 stations were used for the period 1922–98. Indices computed by averaging data from these three groups of stations separately produced very similar results to the 11-station index presented here, indicating that the number of stations used did not affect the results to any significant extent.

TABLE 2. List of meteorological stations used in this study. All data are for 1922–98 (available from NCAR at http://dss.ucar.edu/datasets/ds570.0/data). The locations of the stations are shown in Fig. 2.

Station	Location	Altitude (m)	Missing data
Barnaul	53.26°N, 83.31°E	252	1931–41
Chita	52.05°N, 113.29°E	685	1922–41
Enisejsk	58.27°N, 92.09°E	78	1931–41
Erbogacen	61.16°N, 108.01°E	291	1922–51
Irkutsk	52.16°N, 104.19°E	513	1931–41
Kirensk	57.46°N, 108.04°E	258	1922–41
Kolpasev	58.19°N, 82.54°E	76	1922–51
Krasnojarsk	56.23°N, 93.17°E	194	1922–51
Minusinsk	53.42°N, 91.42°E	254	1922–41
Troickij Priisk	54.6°N, 113.1°E	1310	1922–51
Turuhansk	65.47°N, 87.57°E	32	1922–41

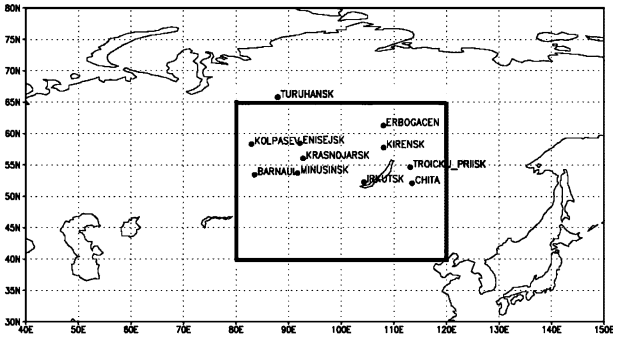

FIG. 2. The location of stations used in this study (for more details see Table 2). The bold rectangle shows the region over which SLP has been averaged to calculate the SH index (40°–65°N, 80°–120°E).

Winter mean (DJF) station-based SHI values were compared with the SHI estimated from the gridded datasets (Fig. 3). All indices were standardized by subtracting the mean and dividing by the standard deviation of the time series. In general, good agreement can be seen between the indices computed from the three gridded datasets. The values of the SHI based on the Trenberth and Paolino (1980) and the GMSLP2 datasets are closest to those of the station-based index (Pearson correlation coefficients are $r = 0.93$ and $r = 0.94$, respectively). By contrast, there is less agreement between the SHI derived from the Jones (1987) dataset and the station-based index ($r = 0.77$).

In addition, the Trenberth dataset has a higher spatial resolution compared to the Jones dataset, and it is continuously updated unlike the GMSLP2 dataset, which has not been updated since 1994. The Trenberth dataset was chosen for further analysis on the basis of all these factors together with the fact that it is widely used in climate variability studies and many errors and discontinuities have been identified and corrected (Trenberth and Paolino 1980). Trends and variability in the intensity of the SH were analyzed using indices derived from the four datasets, however, only the index based on the Trenberth dataset was used in investigation of the SH teleconnectivity.

3. Temporal variability of the SH

a. Trends in the intensity of the SH

Figure 4 shows standardized DJF time series of the SHI derived from the Trenberth dataset (Trenberth

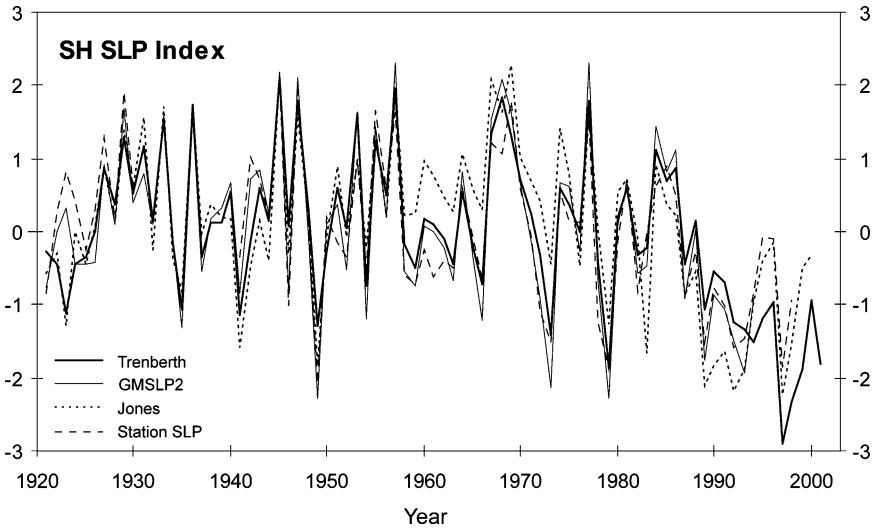

FIG. 3. Standardized winter (DJF) SLP averaged over the area 40°–65°N, 80°–120°E using three different gridded SLP datasets and an average of observations from 11 stations within the same area in Siberia. The standard deviation of the (nonstandardized) station SLP is 2.1 hPa.

and Paolino 1980). A 21-term Henderson filter is used to show longer-term trends (Henderson 1916). This filter smooths the data retaining quadratic and cubic polynomial trends and produces smoother variations than binomial filters (Kenny and Durbin 1982). The main features of the SHI are low values at the beginning of the twentieth century, higher values of SHI in the middle of the twentieth century, and, most importantly, a steep downward trend observed after 1977 (Fig. 4). Means were calculated and plotted for the periods 1900–77 and 1978–2001 to emphasize the different regime in the SH intensity after 1978 (Fig. 4). The steep decline of the SH after 1978 is confirmed by the SHIs derived from all three gridded datasets and also the station data (Fig. 3).

Linear regression has been used to quantify the downward trend in the period 1978–98 and also in the period 1922–98 when all four datasets were available, and the results are summarized in Table 3. The mean downward trend over the period 1978–98 ranges from

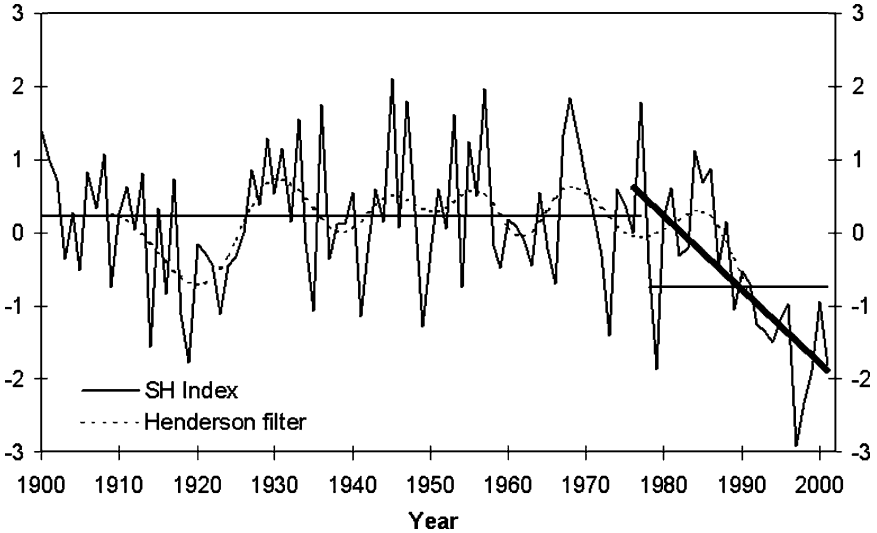

FIG. 4. Standardized winter (DJF) SHI averaged over the area 40°–65°N, 80°–120°E using the SLP dataset (Trenberth and Paolino 1980). The linear trend fit shows the decline in the SH intensity in the period 1978–2001, whereas the 21-order Henderson filter reveals the lower-frequency variability. Means for 1900–77 and 1978–2001 are indicated (horizontal thin lines).

TABLE 3. Linear trend analysis of the SH indices derived from different SLP datasets. The p values refer to testing the null hypothesis that there is no trend in the intensity of the SH. The std error is the standard error in the regression slope, and variance is the amount of total variance of the SH explained by the linear trend.

Dataset	Trend ± std error [hPa (decade)$^{-1}$]	p value	Variance explained (%)
1922–98			
Trenberth	−0.35 ± 0.09	<0.001	20.4
Jones	−0.31 ± 0.12	0.011	8.2
GMSLP2	−0.16 ± 0.09	0.080	4.2
Station SLP	−0.54 ± 0.14	<0.001	21.6
1978–98			
Trenberth	−2.6 ± 0.3	<0.001	41.4
Jones	−2.5 ± 0.3	0.003	36.7
GMSLP2	−1.6 ± 0.6	0.057	20.8
Station SLP	−1.6 ± 0.3	<0.001	31.3

−1.6 hPa decade^{-1} in the GMSLP2 and station datasets to –2.5 hPa decade^{-1} in the Jones dataset and –2.6 hPa decade^{-1} in the Trenberth and Paolino (1980) dataset. The trend is statistically significant at the 1% level in all but the GMSLP2 dataset. In addition, the downward trend accounts for a large amount of total variance in the period 1978–98 reaching 41.4% for the Trenberth data. Unprecedented low values of the SHI have been observed during this period (Fig. 4).

The current weakening of the SH is unprecedented and considerably more than the weakening observed around 1920. A comparison of Fig. 1 depicting SLP averaged over 1900–2001 and Fig. 5a depicting SLP averaged over 1985–2001 shows the weaker mean anticyclone during the most recent 15 yr, with the net pressure decrease over Siberia clearly visible in Fig. 5b. Compensating increases in pressure have occurred over the subtropical Atlantic and south of the Siberian high regions.

b. Possible temperature effects on the trend

The occurrence of the unprecedented downward trend in the last two decades raises questions about the origin of the trend. Figure 6 shows standardized winter (DJF) surface air temperature (SAT) anomalies and SLP averaged over the same area as the SHI domain computed from a set of monthly mean temperatures compiled by Jones et al. (1999) on a 5° × 5° grid. Substantial warming has been observed in this area after 1970 coinciding in time with the strong weakening of the SH. A strong negative correlation of $r = -0.66$ (significantly different from zero at the 1% level) has been found between the two time series.

Trends in SLP over land must be treated carefully because SLP is calculated from surface pressure by using the hydrostatic equation and surface temperature to extrapolate to sea level. It is therefore possible that although the surface pressure of a station remains constant in time, trends may artificially appear in the SLP record of the station because of large trends in temperature. Simple calculations using the hydrostatic equation, used to extrapolate pressure down to sea level, show that the observed warming over Siberia is not sufficient to explain the decrease in SLP without having also a decrease in surface pressure (see the appendix).

In particular, if there were no change in surface pressure over the SHI domain during the period 1922–98, the significant rise in temperature (~3°C) observed in the area over the same period (without any reduction in surface pressure) would result in an SLP decrease of only 0.6 hPa, which is much smaller compared to the 2.8-hPa decrease observed in SLP in the studied area. Similar calculations for the period 1978–98 give an SLP decrease of 0.04 hPa, which contrasts with the observed SLP decrease of 5.2 hPa. With no change in surface

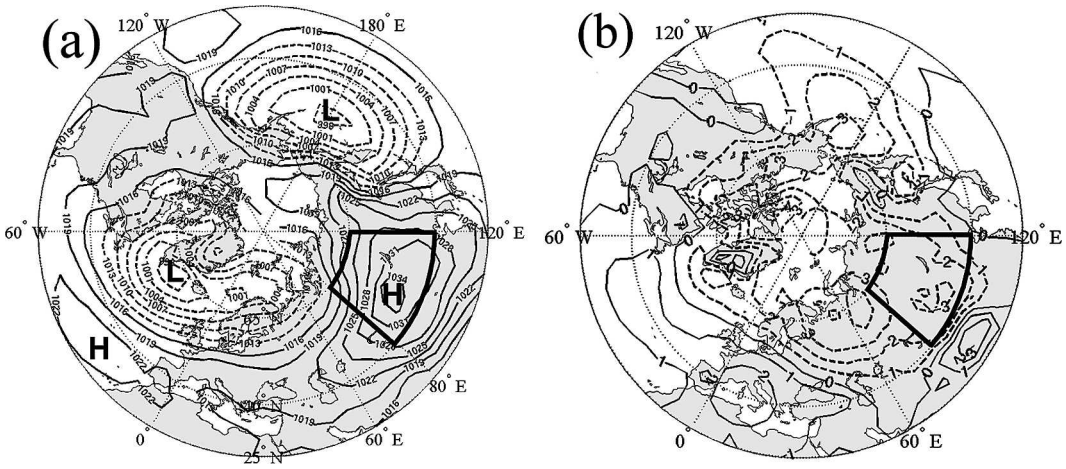

FIG. 5. (a) Winter (DJF) SLP averaged over 1985–2001. (b) The difference between mean SLP shown in (a) and Fig. 1. Contour spacing in (b) is 1 hPa, solid contours represent positive values (SLP increases), and dashed contours are used for negative values (SLP decreases). The area enclosed by the bold line shows the region over which SLP has been averaged to calculate the SHI (40°–65°N, 80°–120°E).

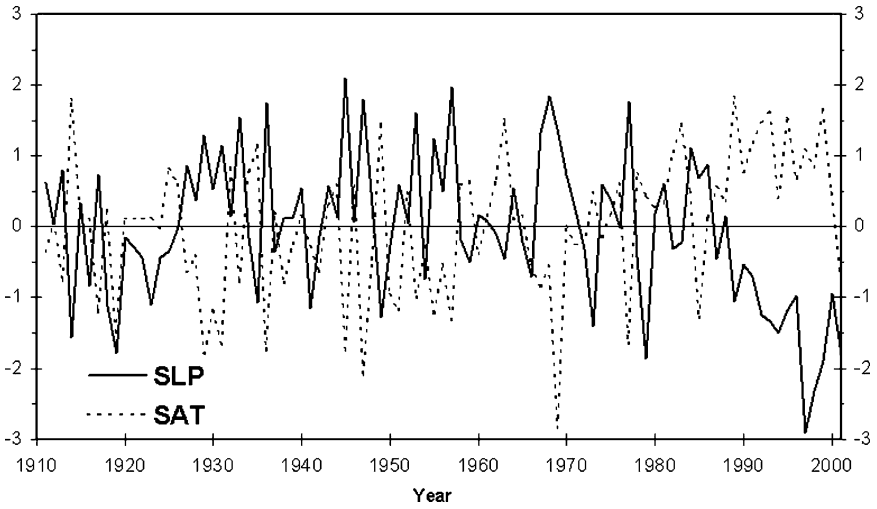

FIG. 6. Standardized winter (DJF) time series of SLP (solid curve; Trenberth and Paolino 1980) and surface air temperature (dashed curve; Jones et al. 1999) anomalies averaged over the area 40°–65°N, 80°–120°E. The standard deviations of (the nonstandardized) SLP and temperature are 2.2 hPa and 2.02°C, respectively.

pressure, temperature increases of 12° and 23°C would be required to explain the observed decreases in SLP over the periods 1922–98 and 1978–98, respectively. The decrease in the SH is therefore not an artifact of the method used to compute SLP from surface pressure.

Analysis of surface pressure data from all available stations (Barnaul, Chita, Enisejsk, Irkutsk, Kirensk, Minusinsk, and Turuhansk; Table 2) confirms that there was a similar change in surface pressure. Figure 7 shows the standardized DJF time series of the SHI obtained by averaging SLP and surface pressure data available from the stations within the area 40°–65°N, 80°–120°E for the period 1922–98. There is a very close agreement between the two indices, and both exhibit low values in the last 30 yr confirming the reliability of the downward trend found in the intensity of the SH.

4. SH teleconnections in the Northern Hemisphere

a. Correlations between the SH index and meteorological fields

The relationships between the SH intensity and other meteorological fields have been investigated by correlating the SHI derived from the Trenberth dataset with this SLP field (Trenberth and Paolino 1980) and various NCEP–NCAR reanalysis fields (Fig. 8). To isolate interannual variations, linear trends have been removed prior to analysis from the SHI and all the fields.

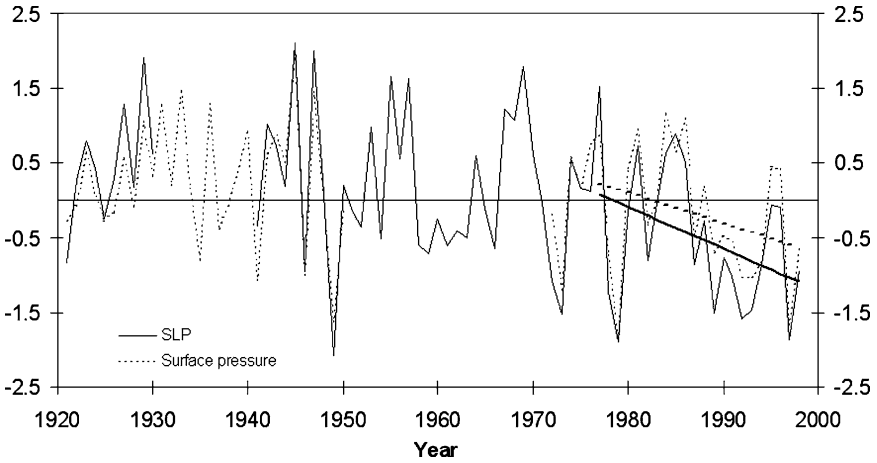

FIG. 7. Standardized winter (DJF) SLP (solid curve) and surface pressure (dashed curve) anomalies averaged using observations from 11 stations within the area 40°–65°N, 80°–120°E.

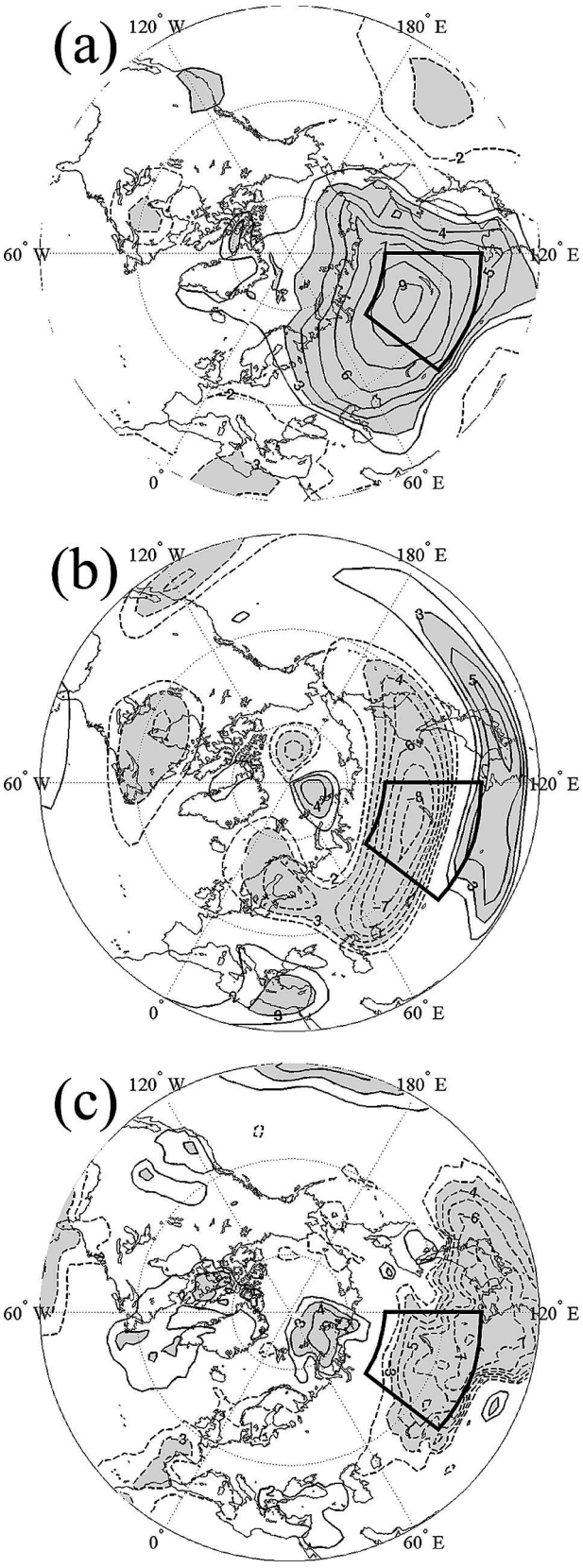

To ensure that the correlations are not due to nonlinear time trends in the data, the analysis has been repeated on the original time series detrended by taking the difference between the value in one year and the previous year, $\Delta z_y = z_y - z_{y-1}$. This is a standard and widely used method for detrending time series (Box and Jenkins 1976; Stephenson et al. 2000). The results (not shown here) are similar to those obtained with only the linear trends removed.

Figure 8a shows the correlations of the SHI with DJF-averaged Trenberth gridded SLP over the period 1899–2001. As expected, an extensive area of strong positive correlations dominates northern Asia extending to southeast China. Negative correlations are observed between the SHI and SLP in the central Mediterranean and Libya and the subtropical part of the North Pacific. These correlations were found to be statistically significant at the 5% level using a two-sample *t* test. The relationship between the SH intensity and pressure over southern Europe implies that enhanced cyclogenesis over the Mediterranean is linked to positive anomalies in SH. This result is in agreement with Rogers (1997), who also linked cyclogenesis in the Mediterranean with a strong SH in his study of the North Atlantic storm-track variability.

Correlations between the SHI and the zonal component of wind at 200 hPa reveal some interesting links between the SH and circulation in the upper troposphere (Fig. 8b). The subtropical jet stream over southeast China and the North Pacific is significantly stronger than usual when the SH is more intense. This intensification of the upper-level winds is a characteristic feature of the East Asian winter monsoon (Cheang 1987). Jhun and Lee (2004) also associated the development of the SH with an enhanced East Asian winter monsoon. The jet stream over the eastern Mediterranean Sea also becomes stronger with the intensification of the SH. By contrast, the upper-tropospheric zonal wind is significantly weaker over northern Asia and northern Europe. Another area of statistically significant positive correlations between the SH and upper-air zonal wind is observed in high latitudes north of the Kara Sea (80°N, 70°E). This suggests that although the SH has largest amplitude in the lower troposphere, it is nonlocally associated with hemispheric-scale upper-tropospheric flow.

←

FIG. 8. Correlation maps showing correlations between the winter (DJF) means of the SHI and (a) SLP for the period 1900–2001 (Trenberth and Paolino 1980), (b) zonal wind (*u*) at 200 hPa, and (c) 2-m temperature for the period 1948–2001 (NCEP–NCAR reanalysis). Correlation coefficients have been multiplied by 10. Solid contours are used for positive correlations and dashed lines are used for negative values. All correlations plotted in (a) are statistically significant at the 5% level using a two-sample *t* test, and gray shading is used for statistically significant correlations at 1% level ($r \geq |0.3|$). Gray shading in (b) and (c) indicates statistical significance at the 5% level ($r \geq |0.3|$).

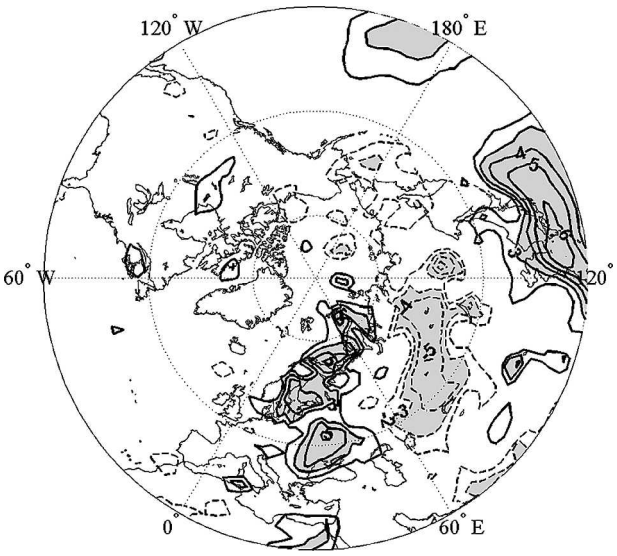

FIG. 9. Correlation map showing correlations between the winter (DJF) SHI and DJF horizontal temperature advection at 1000 hPa. Gray shaded contours represent correlations significant at the 5% level ($r \geq |0.3|$).

The correlations between the SHI and air temperature [2-m temperatures over land and sea surface temperatures (SSTs)] from NCEP–NCAR reanalysis are also well defined in many regions (Fig. 8c). An intense SH is associated with colder than average conditions in the SH area extending downstream to the North Pacific and Southeast Asia. This shows the strong relationship between the SH and the East Asian winter monsoon and the intrusions of cold air into these areas.

Air temperatures and SSTs in the Kara and part of the Laptev sectors of the Arctic exhibit positive correlations with the SH intensity. These can be explained by the advection of warm air from Europe associated with the returning south/southwesterly flow along the SH periphery when the SH is strong. The low-level (1000 hPa) horizontal temperature advection data (T_{adv}) were computed from the NCEP–NCAR reanalyses using centered finite difference approximations to

$$T_{\text{adv}} = -\overline{u}\partial_x\overline{T} - \overline{v}\partial_y\overline{T}, \quad (1)$$

where T is temperature, u is the zonal component, and v is the meridional component of the wind at 1000 hPa and the overbar is the time average for DJF. Correlations between the SHI and the low-level (1000 hPa) horizontal temperature advection confirm this by showing an extensive area of warm advection in eastern and northern Europe reaching the Russian Arctic (Fig. 9). The role of the warm advection is further supported by the fact that the correlation coefficients between temperature in the Kara–Laptev sector of the Arctic and the SHI are significantly larger, reaching $r = 0.7$, in early winter (November and December) when the air masses over Europe are still considerably warmer than the air masses over the Kara–Laptev sector of the Arctic. The positive correlation between these temperatures and the SH may also help explain the observed lack of warming in the Kara–Laptev sector of the Arctic despite the reported increase in low-pressure systems frequency (Shahgedanova and Kuznetsov 2002) and warming projected by general circulation models (GCMs; Manabe and Stouffer 1994). While most GCMs predict that winter air temperatures in these parts of the Arctic should increase considerably (Houghton et al. 2001), no positive trends have been observed since the 1950s (Przybylak 2000), possibly because of reduced southerly advection due to a weakening SH.

The strong relationship between the SHI and horizontal advection of surface temperature over the source area of the SH can help provide further insight on mechanisms of development of the SH. Temperature advection is reduced over Siberia when the SH is strong ($r = -0.5$; Fig. 9). A possible mechanism is as follows: when the anticyclone starts to establish over Siberia, extratropical cyclones are blocked and head farther north over the Kara–Laptev Seas (increasing temperature advection there) and less storms pass over Siberia, thereby decreasing temperature advection. Therefore, an implication of the observed decline of the SH is an increasing passage of storms and associated warm advection over the source area of the SH.

Further support for the important role of the warm advection over northeastern Europe and the Kara–Laptev sector of the Arctic comes from the correlations of the SHI and the meridional component of the wind, which show a strong southerly flow in this area (Fig. 10). Notable are also strong negative correlations over Southeast Asia and the Far East at the surface (Fig. 10c), which suggest a strong link between the SH intensity and the northerly flow along the Pacific rim (the East Asian winter monsoon). There is also clear evidence at 200 and 500 hPa of a well-defined wave train of alternating southerly and northerly flow. The wave train is present through the depth of the troposphere with an equivalent barotropic structure but is better defined in the middle troposphere (Fig. 10b), where its extent from the subtropical North Atlantic to central Siberia is clearly visible. The SH is therefore not simply a local low-level phenomenon.

The relationship between the SH and air temperature at 2 m and SSTs in the Eurasian Arctic and warm advection partly explains variability in the extent of sea ice particularly in the Greenland and Barents Seas where negative correlations of -0.5 are observed (Fig. 11). It is in this region, known as the climatological marginal ice zone (MIZ), that most variability in sea ice extent in winter is confined to (Deser et al. 2000), while the Arctic Seas farther east remain frozen from October to June (Shahgedanova and Kuznetsov 2002). It should be noted, however, that the decline of sea ice extent in this region is also associated with the upward

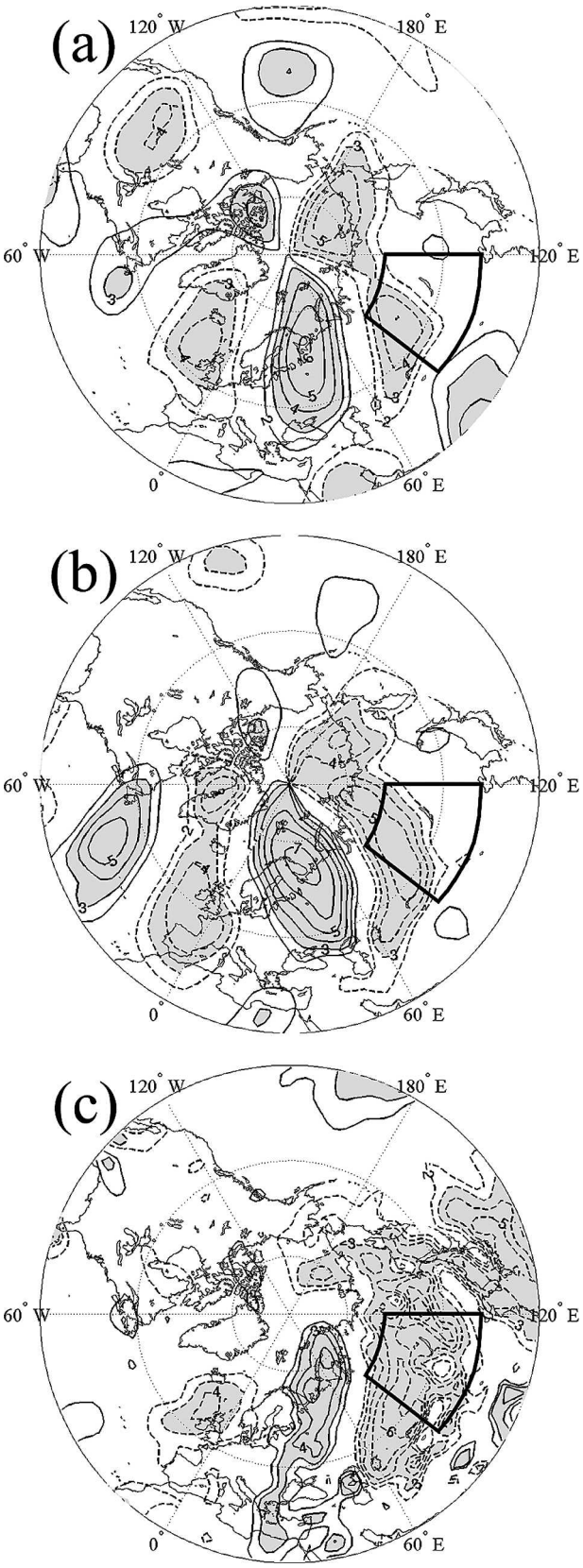

trend in the North Atlantic Oscillation/Arctic Oscillation (NAO/AO; Deser et al. 2000).

Correlations between the SH and precipitation (not shown) are consistent with the associated circulation patterns: drier than normal conditions over a large part of Siberia are associated with a strong SH, while precipitation is enhanced in southeastern Europe.

The correlations between the SHI and meteorological variables are statistically significant at the 5% level in many regions over the period 1948–2001. To confirm the stability of the relationships, correlation analyses have been repeated for the periods 1948–74 and 1975–2001 separately, and results were found to be very similar to those presented here for the whole period.

b. Explanation of the SH in terms of teleconnection pattern indices

A comprehensive review of NH teleconnection patterns (Panagiotopoulos et al. 2002) reveals that despite its importance as a center of action, the SH is not uniquely associated with any robust teleconnection pattern in the NH. This is surprising considering the significant variability in the intensity of the SH and its teleconnections with atmospheric circulation and temperature. It is therefore of interest to examine the relationship between the SH and the main teleconnection patterns in the NH.

Correlation and regression analyses have been used for that purpose using winter mean teleconnection indices obtained from the Climate Prediction Center (CPC; available online at http://www.cpc.ncep.noaa.gov/data/teledoc/telecontents.html). The CPC indices used include the NAO, East Atlantic (EA), Scandinavian (SCA), Polar/Eurasian (POL), West Pacific (WP), East Pacific (EP), East Atlantic/West Russia (EA/WR) and the Pacific–North America pattern (PNA). The AO index (Thompson and Wallace 1998) has also been used (available online at http://jisao.washington.edu/data/annularmodes/Data/ao_index.html). The CPC indices are constructed by taking winter (DJF) averages of monthly standardized amplitudes of rotated principal components of monthly mean 700-hPa geopotential height anomalies for 1951–2000. To avoid spurious effects due to long-term trends, all the teleconnection indices and the SHI were detrended prior to regression and correlation analysis using five-order Henderson filters.

Correlation analysis is first used to assess the relationship between the SH and teleconnection indices.

←

FIG. 10. Correlation maps showing correlation between the winter (DJF) means of the SHI and the meridional component of the wind at (a) 200 hPa, (b) 500 hPa, and (c) 10 m. Gray shaded contours represent correlations significant at the 5% level ($r \geq |0.3|$).

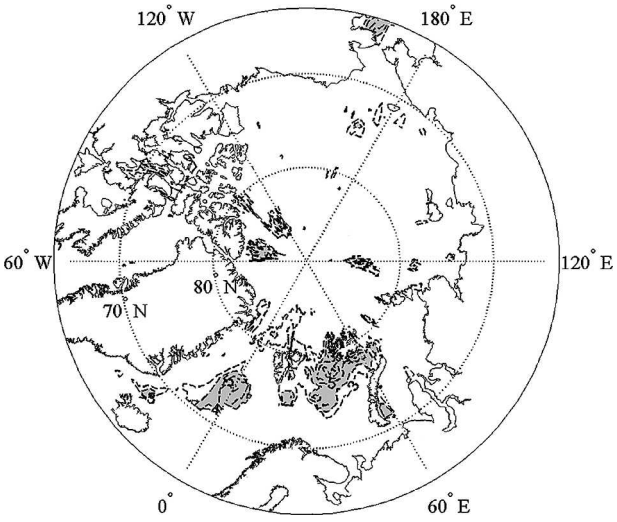

FIG. 11. Correlation map showing correlations between the winter (DJF) means of the SHI and sea ice. Gray shading indicates statistical significance at the 5% level ($r \geq |0.4|$). Sea ice data are the Reynolds ice cover data (version 2) spanning the period 1981–2001 and are available from the National Oceanic and Atmospheric Administration (NOAA).

The effect of autocorrelation or serial correlation in the time series was treated by computing the effective degrees of freedom (37 as opposed to the 48 original degrees of freedom) using the equation given in Zwiers and von Storch (1995). Taking a mean autocorrelation of 0.15 for all indices resulted in an estimated two-sided critical value for statistically significant correlations at the 10% level of $|r| = 0.27$. The AO, POL, and WP are the only indices that have a statistically significant correlation with the SHI at the 10% level, but none of the correlations are statistically significant at the 5% level (Table 4). Jhun and Lee (2004) found that the SH is more strongly correlated with the AO than any other teleconnection pattern, and they pointed out that the correlation increases in interdecadal time scales.

TABLE 4. Correlation coefficients and regression parameter estimates. Columns 2 and 3 show correlation coefficients between the SH and SAT over the source area of the SH and teleconnection indices for DJF. Columns 4 and 5 show parameter estimates (β) from multiple linear regression using teleconnection indices and teleconnection indices plus regional SAT, respectively. One asterisk denotes statistical significance at the 10% level and two asterisks denote significance at the 5% level.

	SH	SAT	β_{tel}	$\beta_{\text{tel}+SAT}$
SH	1	−0.58**	—	—
SAT	−0.58**	1	—	−0.76**
POL	−0.27*	0.45**	−0.35*	0.15
WP	−0.27*	0.02	−0.25	−0.15
SCA	0.13	−0.51**	0.16	−0.31
PNA	0.10	0.10	0.12	0.19
EA/WR	0.06	0.12	0.21	0.11
NAO	0.02	0.22	−0.02	0.16
EA	−0.02	−0.08	0.01	0.04
EP	−0.01	−0.11	0.04	−0.05
AO	−0.29*	0.43**	—	—

Multiple linear regression has been used to account for interannual variability in the intensity of the SH in terms of teleconnection indices and to assess the role of the teleconnection patterns in the decline of the SH observed during 1978–2001. The AO has not been included in the regression model since it is a linear combination of the NAO and POL patterns (http://www.cpc.ncep.noaa.gov/products/precip/CWlink/ao_aao.html). A technique suggested by Junge and Stephenson (2003) has been used whereby the multiple regression coefficients obtained using the detrended indices (Table 4) have been applied to the original trending teleconnection indices. The predicted SH value using all the teleconnection indices does not reproduce the interannual variability or trends well and explains only 13.4% of total variance (Fig. 12a). POL is the only statistically significant predictor at the 10% level explaining alone 6.9% of variance (Table 4).

Inclusion of regional temperature (SAT averaged over 40°–65°N, 80°–120°E; Jones et al. 1999) significantly improved the regression model. The predicted SH value using the teleconnection indices plus regional SAT reproduces both the interannual variability and the decline in the SH and explains 44.4% of total variance (Fig. 12b). Local SAT is the only statistically significant predictor explaining alone 33.9% of variance (Table 4).

5. Conclusions and discussion

This study has investigated variability in the intensity of the SH by carefully defining a robust SH index (SHI) and then using it in correlation and regression studies of meteorological fields and teleconnection indices. The major findings are as follows:

1) A dramatic downward trend of −2.5 hPa decade^{-1} in the SHI occurred between 1978 and 2001. Unprecedented low values of the SHI have been observed in this period. The downward trend was shown to be statistically significant and not due to uncertainties in different datasets or extrapolation of surface pressure to sea level values.
2) Correlations between the SHI and various meteorological fields have shown that the SH affects atmospheric circulation and temperature patterns well outside its source area. Teleconnections between the SH and jet streams and temperature in the western part of the Eurasian Arctic have been established. Advection of warm air from eastern Europe has been identified as the main mechanism causing milder than normal conditions over the Kara and Laptev Seas in association with a strong SH. A link has been found between the SH intensity and sea ice formation in the western Eurasian Arctic. The important role of the SH in the East Asian winter monsoon has also been confirmed.

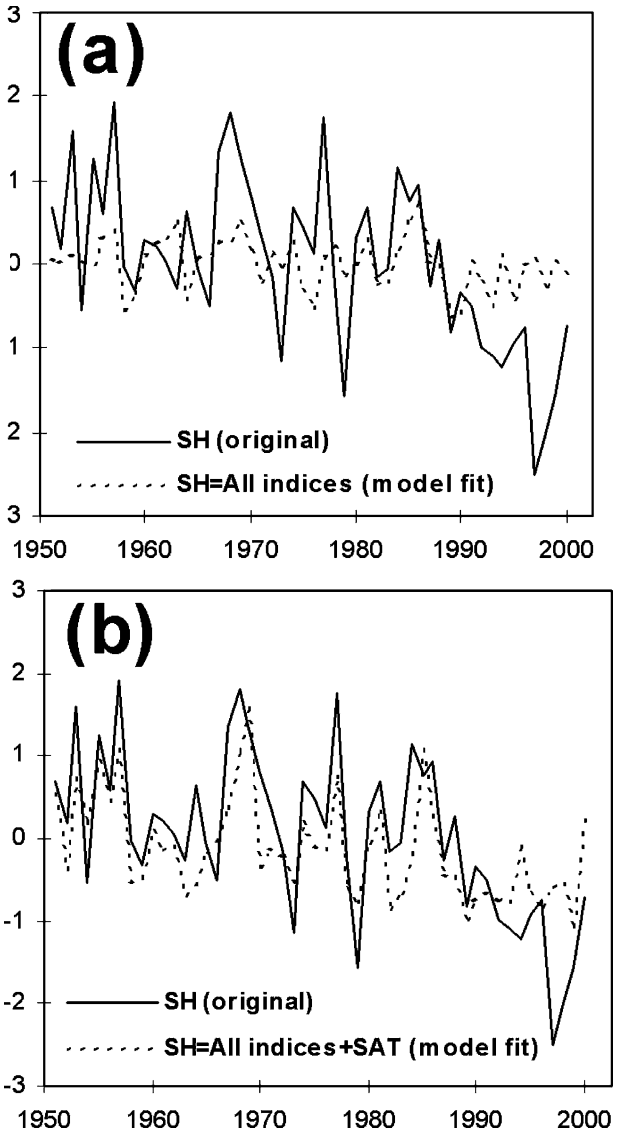

FIG. 12. Time series of winter (DJF) means of the original SH index and the SH index reconstructed from a multiple linear regression model (Table 4) using (a) all teleconnection indices and (b) all indices plus SAT over the source area of the SH.

3) Teleconnection indices alone are not able to reproduce the interannual variability and trends in the SH. Regional SAT has been found to be important in reproducing both interannual variability and the decline in the SH.

While this study has addressed several questions about trends and variability in the SH, it has not clearly discovered what is the cause of the decline in the SH. We have shown that the downward trend is not an artifact of the hydrostatic adjustment of surface pressure to SLP. The SH originates predominantly from the intensive radiative cooling of the surface between October and April, and its intensity correlates closely with surface air temperature (SAT). Therefore, changes in the intensity of radiative cooling can lead to changes in the SH. The strong positive trends in SAT observed over Siberia in recent decades exceed warming at any other location on the globe (Jones et al. 1999; Houghton et al. 2001). However, changes in nonlocal large-scale atmospheric circulation can also have an effect on the intensity of the SH. This study has shown the SH to be weakly related to the AO, POL, and WP teleconnection indices. However, it was also shown that teleconnection indices alone cannot reproduce the downward trend in the intensity of the SH with local temperature playing a more important role.

Future climate projections by GCMs also suggest a decline in the SH in response to increased concentrations of greenhouse gases (Gillett et al. 2003). A preliminary comparison of all available GCMs' future projections of SLP over the source area of the SH (obtained from http://ipcc-ddc.cru.uea.ac.uk) has shown that while there is no close agreement between the models and different scenarios, a clear consensus emerges on the continuation of the observed decline of the SH until 2100.

Acknowledgments. The authors gratefully acknowledge useful discussions with Prof. Brian Hoskins and Dr. Bob Livezey. Part of the analysis has been performed using Climate Explorer at Netherlands's Meteorological Institute (KNMI; available online at http://climexp.knmi.nl). Two anonymous reviewers are also gratefully acknowledged for their detailed and helpful comments and suggestions.

APPENDIX

The Effect of Temperature on the Calculation of SLP

Sea level pressure (p_0) is generally calculated from station pressure (p) measured at height z above sea level by using the hydrostatic equation,

$$p = p_0 e^{-(z/H)}, \tag{A1}$$

where H is the pressure scale height. For an isothermal atmosphere, the scale height is given by $H = RT/g$, where R is the gas constant for dry air, T is the surface air temperature, and g is the global mean acceleration due to gravity at the earth's surface.

The change in p_0 over a period of time can be calculated by differentiating (A1):

$$\frac{\Delta p}{p_0} \approx \frac{\Delta p_0}{p_0}\left(1 - \frac{z}{H}\right) + \frac{z}{H}\frac{\Delta T}{T}. \tag{A2}$$

If it is assumed that no change took place in the surface pressure p (i.e., $\Delta p = 0$), and suitable values for the period 1920–98 are chosen ($z = 400$ m, $T = 253$ K, and $p_0 = 1031$ hPa), then a warming (ΔT) of 3 K would result in $\Delta p_0 = -0.7$ hPa compared to the observed

decrease in SLP of 2.8 hPa over the same period. The corresponding value for the period 1978–98 is 0.04 hPa compared to the observed 5.2 hPa.

Using (A2), it can be estimated that a temperature rise of 12° and 23°C would be needed to justify alone the observed decreases in SLP over the periods 1922–98 and 1978–98, respectively, without proportional decreases in surface pressure.

REFERENCES

Allan, R., J. Lindesay, and D. E. Parker, 1996: *El Nino Southern Oscillation and Climatic Variability*. CSIRO, 416 pp.

Box, G. E. P., and G. M. Jenkins, 1976: *Time Series Analysis: Forecasting and Control*. Holden-Day, 575 pp.

Cheang, B.-K., 1987: Short- and long-range monsoon prediction in Southeast Asia. *Monsoons*, J. S. Fein and P. L. Stephens, Eds., John Wiley, 579–606.

Clark, M. P., M. C. Serreze, and D. A. Robinson, 1999: Atmospheric controls on Eurasian snow extent. *Int. J. Climatol.,* **19,** 27–40.

Cohen, J., and D. Entekhabi, 1999: Eurasian snow cover variability and Northern Hemisphere climate predictability. *Geophys. Res. Lett.,* **26,** 345–348.

Deser, C., J. E. Walsh, and M. S. Timlin, 2000: Arctic sea ice variability in the context of recent atmospheric circulation trends. *J. Climate,* **13,** 617–633.

Gillett, N. P., F. W. Zwiers, A. J. Weaver, and P. A. Stott, 2003: Detection of human influence on sea-level pressure. *Nature,* **422,** 292–294.

Henderson, R., 1916: Note on graduation by adjusted average. *Trans. Amer. Soc. Actuar.,* **17,** 43–48.

Houghton, J. T., Y. Ding, D. J. Griggs, M. Noguer, P. J. van der Linden, X. Dai, K. Maskell, and C. A. Johnson, Eds., 2001: *Climate Change 2001: The Scientific Basis*. Cambridge University Press, 881 pp.

Jhun, J. G., and E. J. Lee, 2004: A new East Asian winter monsoon index and associated characteristics of the winter monsoon. *J. Climate,* **17,** 711–726.

Jones, P. D., 1987: The early twentieth century Arctic High—Fact or fiction? *Climate Dyn.,* **1,** 63–75.

——, M. New, D. E. Parker, S. Martin, and I. G. Rigor, 1999: Surface air temperature and its changes over the past 150 years. *Rev. Geophys.,* **37,** 173–199.

Junge, M. M., and D. B. Stephenson, 2003: Mediated and direct effects of the North Atlantic Ocean on winter temperatures in northwest Europe. *Int. J. Climatol.,* **23,** 245–261.

Kenny, P., and J. Durbin, 1982: Local trend estimation and seasonal adjustment of economic and social time series. *J. Roy. Stat. Soc.,* **145A,** 1–41.

Lydolf, P. E., 1977: *Climates of the Soviet Union*. Elsevier, 443 pp.

Manabe, S., and R. J. Stouffer, 1994: Multiple-century response of a coupled ocean–atmosphere model to an increase of atmospheric carbon dioxide. *J. Climate,* **7,** 5–23.

Mokhov, I. I., and V. K. Petukhov, 1999: Atmospheric centers of action and tendencies of their change. *Izv. Acad. Sci. USSR, Atmos. Oceanic Phys.,* **36,** 292–299.

Panagiotopoulos, F., M. Shahgedanova, and D. B. Stephenson, 2002: A review of Northern Hemisphere winter-time teleconnection patterns. *J. Phys. IV*, **12,** 1027–1047.

Przybylak, R., 2000: Temporal and spatial variation of surface air temperature over the period of instrumental observations in the Arctic. *Int. J. Climatol.,* **20,** 587–614.

Rogers, J. C., 1997: North Atlantic storm track variability and its association to the North Atlantic Oscillation and climate variability of northern Europe. *J. Climate,* **10,** 1635–1647.

Sahsamanoglou, H. S., T. J. Makrogiannis, and P. P. Kallimopoulos, 1991: Some aspects of the basic characteristics of the Siberian anticyclone. *Int. J. Climatol.,* **11,** 827–839.

Shahgedanova, M., and M. Kuznetsov, 2002: The Arctic environments. *The Physical Geography of Northern Eurasia*, M. Shahgedanova, Ed., Oxford University Press, 70–102.

Stephenson, D. B., V. Pavan, and R. Bojariu, 2000: Is the North Atlantic Oscillation a random walk? *Int. J. Climatol.,* **20,** 1–18.

——, H. Wanner, S. Brönnimann, and J. Luterbacher, 2002: The history of scientific research on the North Atlantic Oscillation. *The North Atlantic Oscillation: Climate Significance and Environmental Impact, Geophys. Monogr.*, No. 134, Amer. Geophys. Union, 37–50.

Thompson, D. W. J., and J. M. Wallace, 1998: The Arctic Oscillation signature in the wintertime geopotential height and temperature fields. *Geophys. Res. Lett.,* **25,** 1297–1300.

Trenberth, K. E., and D. A. Paolino, 1980: The Northern Hemisphere sea-level pressure data set: Trends, errors, and discontinuities. *Mon. Wea. Rev.,* **108,** 855–872.

Zwiers, F. W., and H. von Storch, 1995: Taking serial correlation into account in tests of the mean. *J. Climate,* **8,** 336–351.